Electrical and plasma characterization of a hybrid plasma source combined with inductively coupled and capacitively coupled plasmas for O atom generation

Kwan-Yong Kim, Kyung-Hyun Kim, Jun-Hyeon Moon, and Chin-Wook Chung[a] (iD)

AFFILIATIONS

Department of Electrical Engineering, Hanyang University, Seoul 04763, South Korea

[a]Author to whom correspondence should be addressed: joykang@hanyang.ac.kr

ABSTRACT

We developed a hybrid plasma source combined with an inductively coupled plasma (ICP) antenna and a capacitively coupled plasma (CCP) electrode. The ICP antenna and the CCP electrode are connected to a single RF power generator in parallel and a variable capacitor C_v is connected to the ICP antenna in series. The currents flowing through each source and the CCP electrode voltage are measured for analysis of the electrical characteristics, and the ion densities are measured while adjusting the capacitance of the C_v. Interestingly, when a series LC resonance occurs between the inductance of the ICP antenna and the capacitance of the C_v, different trends are observed depending on the discharge mode. In capacitive mode (E-mode), the ion density is minimized and is controlled by the CCP current. On the other hand, in inductive mode (H-mode), the ion density is maximized and is affected by the ICP current. The change of the ion density can be explained by the balance between the total power absorption and power dissipation. It is also in good qualitative agreement with the calculated plasma density from the power balance equation. By adjusting the C_v, linear control of the ion density can be achieved. To evaluate the proposed source in terms of O atom generation, the number density ratio of O atom n_O to Ar n_{Ar} is obtained by using the optical emission spectroscopy actinometry method. These results show that n_O/n_{Ar} is controlled. Our source can be applied to plasma processing, in which ion density and O atom generation controls are important factors.

Published under license by AIP Publishing. https://doi.org/10.1063/5.0006417

I. INTRODUCTION

Inductively coupled plasmas (ICPs) have attractive characteristics, such as generating high ion density ($n_i > 10^{11}$ cm^{-3}) and a relatively simple structure.[1–3] However, ICPs cannot generate the linear ion density due to the E-mode (capacitive coupling) to H-mode (inductive coupling) transition.[4–6] The capacitively coupled plasmas (CCPs) generate relatively low ion density ($n_i < 10^{10}$ cm^{-3}), but they can be able to linearly control ion density with RF power.[7–9] Nowadays, two or more plasma sources can be combined to utilize the advantages of each source. These sources are called hybrid sources and these hybrid sources have been studied because of its advantages compared to single plasma sources. Hybrid sources have been studied for plasma parameter control. The ion density and ion energy are controlled by the RF power and the DC bias power in DC–RF hybrid source.[10] High ion density has been achieved while independently controlling ion energy in ECR–RF hybrid source.[11] The microwave–RF

hybrid source was studied in terms of the control of ion energy distribution and ion flux.[12] However, all of the hybrid source requires a power generator and a matching system for each source.

As semiconductor manufacturing processes become more complex,[13–15] sophisticated ion density and radical control become increasingly important.[16–19] When the E- to H-mode transition occurs in ICP, the ion density suddenly increases from low- to high-density. This phenomenon limits linear ion density control. In addition, hybrid sources generally require multiple power generators. Therefore, a new type of hybrid plasma source that can overcome these disadvantages is required.

In this work, we develop a hybrid plasma source combining ICP and CCP with variable capacitor connected to the ICP antenna. By adjusting capacitance, the current flowing to each source is controlled. Electron temperature and ion density are measured using the floating harmonic method (FHM),[20] and the electrical properties of voltage

and current are measured by a voltage probe and current probes, respectively. When the series LC resonance between the variable capacitor and the inductance of the ICP antenna occurs, different trends are observed in each discharge mode. In E-mode, the ion density is controlled by the CCP electrode current. In contrast, in H-mode, the ion density is controlled by the ICP current. Furthermore, linear control of the ion density is achieved by adjusting the capacitance of the variable capacitor C_v. In order to evaluate the proposed source in terms of O atom generation control, the number density ratio of O to Ar is obtained from the optical emission spectroscopy (OES) actinometry method. By adjusting the current flowing through each source with the variable capacitor, the ion density can be precisely controlled, which is a significant and important advantage of the proposed hybrid plasma source.

II. EXPERIMENTAL SETUP AND MEASUREMENTS

Figure 1 shows a schematic of the experimental setup. The top and bottom of the cylindrical reactor are made of stainless steel, and the side of the reactor is made of quartz. The height and the inner diameter of the reactor are 12 cm and 16.8 cm, respectively. The diameter of the CCP electrode is 9 cm, and its surface is covered with ceramic (Al_2O_3) to prevent sputtering. A variable capacitor is connected in series with a one-turn ICP antenna, and its variable capacitance range is from 50 to 550 pF. Current probes (110, Pearson Electronics Inc.) are installed between the matching box (Path Finder, PLASMART Inc.) and the hybrid plasma source. The measured currents are used to calculate the system resistance R_s and to investigate the current flowing to each source. A voltage probe (P5100, Tektronix Inc.) is mounted onto the powered line to measure the CCP electrode voltage. The current probes and the voltage probe were connected to an oscilloscope (DSOX2014A, Keysight). The system resistance R_s is

FIG. 1. Schematic diagram of the hybrid plasma source.

the sum of the circuit resistance of the matching box and the hybrid plasma source. R_s is obtained by $R_s = P_{rf}/I_{rf}^2$, when the plasma is turned off,[21,22] where P_{rf} and I_{rf} are the applied RF power and the current flowing through the hybrid plasma source system, respectively. R_s varies from 0.14 to 0.24 Ω depending on the capacitance of the variable capacitor C_v. When the plasma is turned on, the applied RF power is consumed by both the hybrid plasma source and the plasma. The absorbed power P_{abs}, which is consumed by the plasma, can be described by the relationship between P_{abs} and P_{rf}, which is given as $P_{abs} = P_{rf} - I_{rf}^2 R_s$. RF power at 13.56 MHz frequency is applied using RF power generator (R601, SEREN IPS Inc.) and the reflection of the RF power is maintained under 1%. Argon and oxygen gases are fed through the top of the chamber from the same gas line, with the flow rates of argon and oxygen set to 10 and 20 sccm, respectively. The base pressure is 6.6×10^{-3} Pa (5×10^{-2} mTorr), and the pumping system includes a rotary oil pump and a turbo molecular pump. The experimental pressures are fixed at 1.33 and 13.3 Pa (10 and 100 mTorr). A planar type floating probe is used to obtain the electron temperature (T_e) and the ion density (n_i) by FHM, and this probe is placed at the center of the chamber. Assuming that the electrons are in the Maxwellian distribution. In addition, this method is also applicable to the non-Maxwell distribution since electrons at the floating potential V_f in the non-Maxwellian distribution form a Maxwellian distribution.[23] The electron temperature is given as follows:

$$T_e \approx \frac{v_0}{4} \frac{I_\omega}{I_{2\omega}}, \tag{1}$$

where I_ω, $I_{2\omega}$, and v_0 are the amplitude of the first harmonic current, the amplitude of the second harmonic current, and the amplitude of the applied sinusoidal voltage, respectively.

The ion density can be found from the amplitude of the first harmonic current as follows:

$$n_i = \frac{I_\omega}{2(0.61 e u_B A_p)} \frac{I_0(v_0/T_e)}{I_1(v_0/T_e)}, \tag{2}$$

where e, u_B, A_P, $I_0(v_0/T_e)$, and $I_1(v_0/T_e)$ are the electron elementary charge, the Bohm velocity, the probe area, and the zero and first order of the modified Bessel functions, respectively.

III. EQUIVALENT CIRCUIT OF THE HYBRID PLASMA SOURCE

Figure 2 shows the equivalent circuit of the hybrid plasma source. The ICP section consists of a one-turn ICP antenna connected to the C_v in series. The CCP section is composed of the CCP electrode. The RF current flows into the ICP and CCP sections, and the current ratio
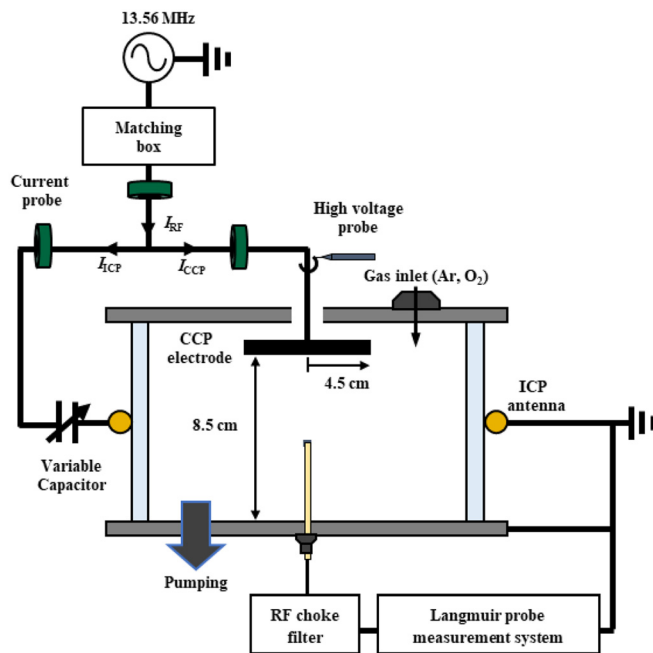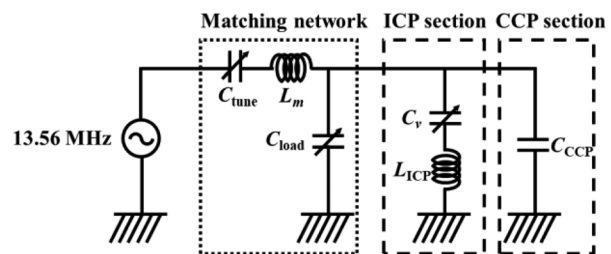

FIG. 2. The equivalent circuit of the hybrid plasma source.

flowing through each source can be controlled by C_v. The total impedance of the hybrid plasma source Z_T, the impedance of the ICP section Z_{ICP}, and the CCP section Z_{CCP} are determined by

$$Z_T = \frac{Z_{ICP}Z_{CCP}}{Z_{ICP} + Z_{CCP}},$$
$$Z_{ICP} = \omega L_{ICP} - (\omega C_v)^{-1}, \tag{3}$$
$$Z_{CCP} = (\omega C_{CCP})^{-1},$$

where L_{ICP}, C_{CCP}, and ω are the inductance of the ICP antenna, the capacitance of the CCP electrode, and the angular frequency, respectively. The L_{ICP} ($\sim$0.98 μH) and the C_{CCP} ($\sim$19.5 pF) were measured by a network analyzer. The series LC resonance $(f = 1/2\pi\sqrt{L_{ICP}C_v})$ of the ICP section occurs at $C_v = 141$ pF without plasma. The current flowing through each source is proportional to its relative impedance and can be expressed by

$$I_{ICP} = (Z_{ICP}/Z_T) \times I_{RF},$$
$$I_{CCP} = (Z_{CCP}/Z_T) \times I_{RF}, \tag{4}$$

where I_{ICP}, I_{CCP}, and I_{RF} are the ICP antenna current, the CCP electrode current, and the output RF current from the matching network, respectively. Thus, the current flowing in each section can be controlled.

IV. EXPERIMENTAL RESULTS AND DISCUSSION
A. Electrical characteristics of the hybrid plasma source

Figure 3 shows that the electrical characteristics depend on C_v at 1.33 Pa (10 mTorr) and 13.3 Pa (100 mTorr). When the series LC resonance occurs in the ICP section, the impedance of the ICP section is nearly zero. In this situation, I_{ICP} is maximized, and I_{CCP} is minimized. The red dashed line in Fig. 3 represents an LC resonance point at a C_v of 148 pF. At this C_v value, I_{CCP} are minimized in both pressures. However, when 300 W RF power is applied at a 1.33 Pa (10 mTorr) neutral pressure, I_{ICP} is maximized at 159 pF (green dashed line) and the LC resonance is shifted from the previous resonance point. This phenomenon can be explained by the transformer circuit model of an ICP, as shown in Fig. 2.[24] The equivalent inductance L_1 is the sum of the inductance of the primary (antenna) and a negative inductance term that represents the total reactance of the coupled secondary (plasma). It can be written as

$$L_1 = L_0 - \frac{\omega M^2[\omega L_2 + (\omega/\nu_{en})R_2]}{R_2^2 + [\omega L_2 + (\omega/\nu_{en})R_2]^2}, \tag{5}$$

where L_0, M [$= k(L_0 L_2)^{1/2}$, where k is the coupling coefficient], L_2 ($= \mu_0\pi R^2/l$, where μ_0, R, l are the permeability of the free space, the radius of the reactor, and the length of the reactor, respectively), ν_{en}, and R_2 ($= \delta_p/\nu_{en}$, where δ_p is the skin depth) are the inductance of the primary antenna coil, the mutual inductance, the geometric inductance, the effective electron collision frequency, and the secondary resistance, respectively. In the experimental condition, we obtained by calculating δ_p and ν_{en}.[25] At 1.33 Pa (10 mTorr), δ_p is a collisionless skin depth, $\delta_{p,l}$, given by $\delta_{p,l} = (m/e^2\mu_0 n_0)^{1/2}$. At this pressure $\delta_{p,l}$ is 0.77 cm and ν_{en} is 34.1 MHz. At 13.3 Pa (100 mTorr), δ_p is the collisional skin depth $\delta_{p,h}$ [$= (2m\nu_{en}/\omega\mu_0 n_0)^{1/2}$], which is 2.19 cm. ν_{en} is 340.8 MHz. L_1 is calculated from the parameters obtained under

experimental conditions. When C_v is 159 pF, the series LC resonance in the ICP section occurs at L_1 of 0.87 μH. The calculated L_1 is 0.9 μH at 1.33 Pa (10 mTorr), so the calculation is in good agreement with the LC resonance condition. Also, I_{CCP} and V_{CCP} at this point are almost the same as the CCP current and voltage at 148 pF. At 13.3 Pa (100 mTorr), the observed I_{ICP} trend is different from that at 1.33 Pa (10 mTorr). As the applied RF power is increased, the maximum I_{ICP} is measured at a C_v value before the LC resonance point. Interestingly, despite these changes, I_{CCP} and V_{CCP} are minimized at 148 pF for all applied powers. This result indicates that the LC resonance point does not move. At above 150 W, I_{ICP} suddenly decreased at 135 and 148 pF. In addition, at 13.3 Pa (100 mTorr), ν_{en} becomes approximately 10 times larger than it was at 1.33 Pa (10 mTorr) and is proportional to R_2. As a result, L_0 and L_1 are almost the same and the LC resonance point does not change. The dependence of the LC resonance point on the pressure is observed. Figures 3(c) and 3(f) show V_{CCP} as changing C_v in both pressures. It is observed that the V_{CCP} follows the same trend as the I_{CCP}. As the applied power increases, the V_{CCP} dramatically changes, depending on the C_v. In general, a high CCP electrode voltage is a disadvantage in plasma generation because it causes ion energy loss. However, our proposed source provides the advantages of a high breakdown voltage of above 13.3 Pa (100 mTorr) for plasma processing application, such as ashing and cleaning. In order to discharge the plasma at the high pressures [$p \geq 13.3$ Pa (100 mTorr)], a high breakdown voltage is required.[26] Generally, an ignition system is installed in the high-pressure processing chamber and the plasma is discharged using its spark. There is a disadvantage in that the ignition circuit corrodes due to the spark generating particles that are highly problematic.[27] In contrast, our source does not require an ignition system; it can easily be discharged by the high electric field of the CCP electrode. By installing C_v as an additional control knob, the currents and voltage can be controlled at a fixed RF power. The electrical characteristics of the hybrid source are the currents and voltage flowing through each source, which can be controlled by adjusting the C_v at a fixed applied power. This feature is an advantage of the hybrid plasma source.

B. Ion density control of the hybrid plasma source

In an ICP discharge, there are E (capacitive coupling) and H (inductive coupling) modes, which can be distinguished by the light emission intensity of the plasma. In addition, it can also be described from comparing the skin depth δ and chamber radius R.[26] If the skin depth is longer than the chamber radius ($\delta > R$), the capacitive coupling is dominant, in E-mode. On the other hand, when the skin depth is shorter than the chamber radius ($\delta < R$), the plasma is mainly affected by the inductive coupling in H-mode.[28,29] When the ion density is 2×10^{10} cm^{-3} ($\delta_p = 7.7$ cm) at 1.33 Pa (10 mTorr) or is 3×10^{10} cm^{-3} ($\delta_p = 7.9$ cm) at 13.3 Pa (100 mTorr), R and δ_p are almost the same length according to the transition density at each pressure condition. In our experiment, we can distinguish between E and H modes based on the transition density value (gray dashed line). Figure 4 shows the ion densities as a function of C_v from 50 to 300 W at 1.33 Pa (10 mTorr) and 13.3 Pa (100 mTorr). At 50 W in 1.33 Pa (10 mTorr) and below 75 W at 13.3 Pa (100 mTorr), these ion densities are lower than the transition density. Although the pressure conditions are different, the same trend is observed as for the I_{CCP}. In E-mode, the CCP electrode voltage is applied to the sheath so that the RF power can be more efficiently transferred to the plasma than the
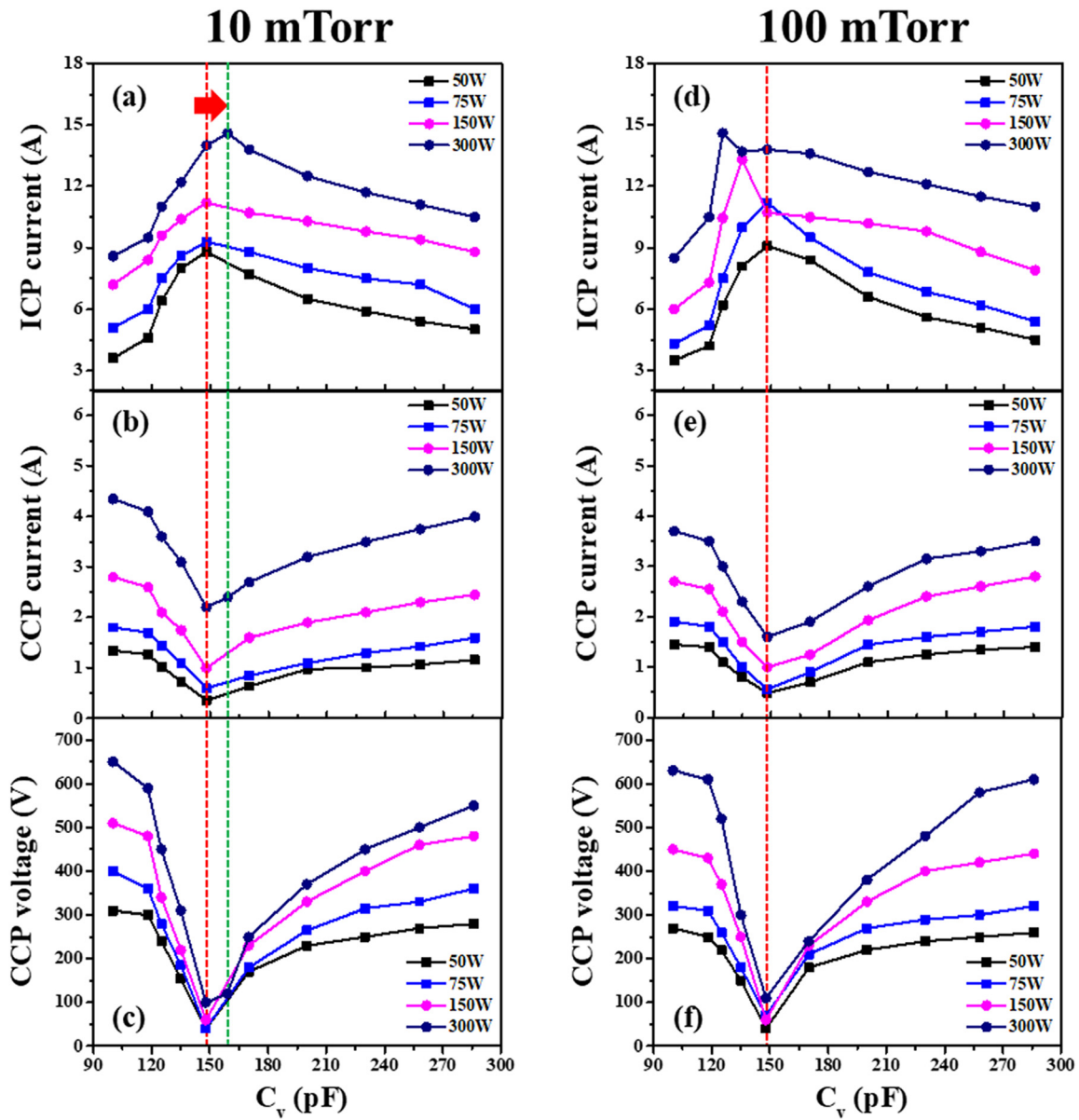
FIG. 3. Measured (a) ICP antenna and (b) CCP electrode currents and (c) CCP voltages at 1.33 Pa (10 mTorr), and (d)–(f) these same measurement at 13.3 Pa (100 mTorr) as a function of C_v.

ICP antenna. Therefore, the ion density is controlled by the I_{CCP}. Above an applied power of 75 W at 1.33 Pa (10 mTorr), the ion densities show a trend similar to that of the I_{ICP} at the same pressure conditions. This result indicates that ion density is controlled by the I_{ICP} in H-mode. Interestingly, at 150 W and 13.3 Pa (100 mTorr), both I_{ICP} and I_{CCP} trends are observed based on the transition density. Before the LC resonance point, the ion density decreased, as with the I_{CCP}, and then suddenly increased near the LC resonance. At this time, the I_{ICP} is suddenly decreased, as shown in Fig. 3(d). This phenomenon is due to an effect of multistep ionization and ion acceleration loss that is decreased by the V_{CCP} during the E to H mode transition.[30,31] At

300 W, the ion densities are maximized at the LC resonance at both pressures. In the H-mode, the high ion density is maintained despite the high V_{CCP} at both ends of the C_v, because the sheath voltage of the CCP electrode is decreased in the high density. Consequently, different ion density trends are observed depending on the plasma driven mode. A conventional single source controls ion density by varying the applied power. However, our source can be elaborately controlled to a wide range of ion densities via the external variable capacitor.

According to the experimental results, the ion density is controlled by I_{CCP} in E-mode and by I_{ICP} in H-mode. This phenomenon
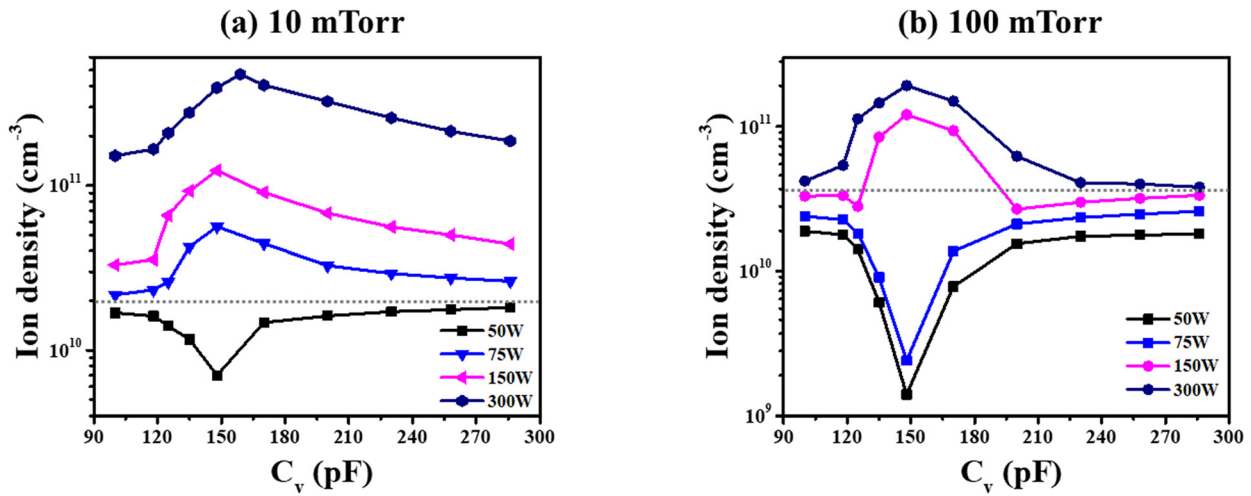
FIG. 4. Ion densities as a function of C_v at various applied powers at (a) 1.33 Pa (10 mTorr) and (b) 13.3 Pa (100 mTorr).

can be understood by using the global power balance model,[25] as follows:

$$n_0 = \frac{P_{abs}}{e u_B A_{eff} \varepsilon_T}, \qquad (6)$$

$$\varepsilon_T = \varepsilon_e + \varepsilon_i + \varepsilon_c, \qquad (7)$$

where n_o, P_{abs}, e, u_B, A_{eff}, and ε_T are the plasma density, the absorbed power of the plasma, the elementary electron charge, the Bohm velocity, the effective area for particle loss, and the total energy loss, respectively. Here, ε_T is a function of the electron temperature and is the sum of the mean kinetic energy lost per ions (ε_i), electrons (ε_e), and the collisional energy loss (ε_c) per electron–ion created. The voltage of the CCP electrode V_{CCP}, which is proportional to ε_i, changes significantly with C_v and is an important parameter that can control the ion density by adjusting the ion energy loss. The plasma density is calculated for each driven mode at both pressures using the global power balance equation, Eqs. (6) and (7). Figure 5 shows the normalized measured ion density and calculated plasma density from a global power balance model at 1.33 Pa (10 mTorr) and 13.3 Pa (100 mTorr), when the applied powers are 50 W and 300 W. Here, the ion density and calculated plasma density profiles were normalized relative to the maximum density. The calculated plasma densities are in good quantitative agreement with the measured values. These results indicate that the plasma is absorbed mostly by the transferred power from the CCP electrode in the E-mode (50 W) and is absorbed dominantly by the transferred power from the ICP antenna in the H-mode (300 W).[32] In contrast, the calculated plasma densities show a large discrepancy with the ion densities at 300 W. The reason is that V_{CCP} caused the huge ion acceleration loss at the CCP electrode, which is proportional to the ε_i, and was largely changed depending on C_v. Therefore, the ion density decreased considerably near 100 pF and 300 pF where the V_{CCP} is large. On the other hand, ε_T in Eq. (6) is significantly smaller than V_{CCP}. When $T_{e,p}$ changes from 2.2 eV at 10 mTorr to 1.5 eV at 100 mTorr, ε_T changes from 52 V to 67 V, where $T_{e,p}$ is the calculated electron temperature based on the particle balance equation.[25] Under this

condition, ε_T is substantially changed small compared to V_{CCP}, so it is negligible. Thus, there is a large discrepancy between the absolute value of the measured ion density and the calculated plasma density.

In a conventional ICP source, the ion density cannot be linearly controlled at an intermediate pressure [$p \leq 6.65$ Pa (50 mTorr)] because a density jump occurs due to the E to H mode transition. However, using our plasma source, the ion density can be linearly generated. Because the CCP electrode voltage is appropriately controlled by adjusting the C_v value, this effect indicates that power dissipation through ion acceleration at the CCP electrode can also be controlled. Figure 6(a) shows that the various combinations of applied powers and C_v can control ion densities through a wide range from low to high density. Low density control (combination 1) consists of low applied powers (50–100 W) and C_v in the 148–258 pF range. This combination can control the ion density in units of 7×10^9 cm^{-3}. Intermediate density control (combination 2) consists of intermediate and high applied powers (150–300 W) and control of C_v within the range of 285–147 pF. This set of parameters can adjust the ion density in units of 4×10^{10} cm^{-3}. High density control (combination 3) consists of high applied powers (200–300 W) and a C_v range of 100–148 pF, which can control the ion density in units of 3×10^{10} cm^{-3}. Interestingly, the density jump-up is not observed, which is one of the strong features of our source. The ion energy flux is also linearly controlled under each of the three conditions, as shown in Fig. 6(b). The ion energy flux (E_{Γ_i}) can be calculated from the ion flux and the sheath voltage as follows:

$$E_{\Gamma_i} = e\Gamma_i V_s \approx 0.8(e\Gamma_i V_{CCP}), \qquad (8)$$

where Γ_i is the ion flux obtained from the FHM[20] and V_s is the sheath voltage at the CCP electrode. Since the hybrid plasma source is an asymmetric CCP source because the ground area of the reactor is approximately four times larger than the CCP area, V_{CCP} is mostly applied to the CCP electrode sheath. Here, the sheath voltage is about $0.8 V_{CCP}$[25] and the unit for the ion energy flux is mW/cm^2. The ion energy flux is obtained under each experimental condition.
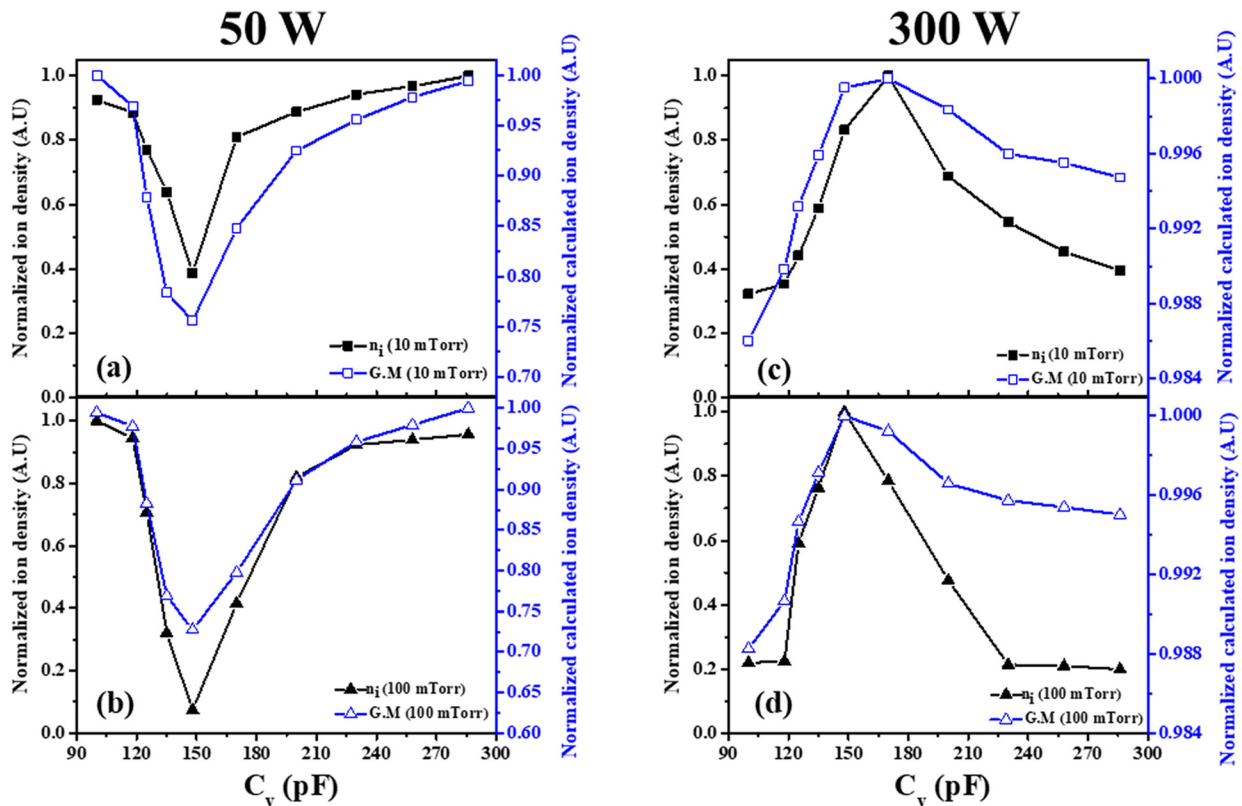
FIG. 5. (a) Normalized measured ion density and calculated ion density from the global model as a function of C_v at 1.33 Pa (10 mTorr) and 13.3 Pa (100 mTorr) using applied powers of (a) and (b) 50 W (E-mode) and (c) and (d) 300 W (H-mode).

Combination 1 is in the low density region, for which the same trends were observed in the ion energy flux and ion density. However, combinations 2 and 3 show the opposite trends in ion energy flux and ion density. In the case of combination 3, the ion energy flux can be adjusted in a wide range of 600–1500 mW/cm^2 while maintaining a high ion density. Using our plasma source, the ion density can be linearly and precisely generated with various combinations. Further, our

source can be effectively applied to plasma processing for which ion density control is an important factor.

C. Oxygen plasma

O$_2$ and Ar are injected at 20 sccm (95.3%) with 1 sccm (4.7%) of a trace rare gas (TRG) for optical emission actinometry. The ion density
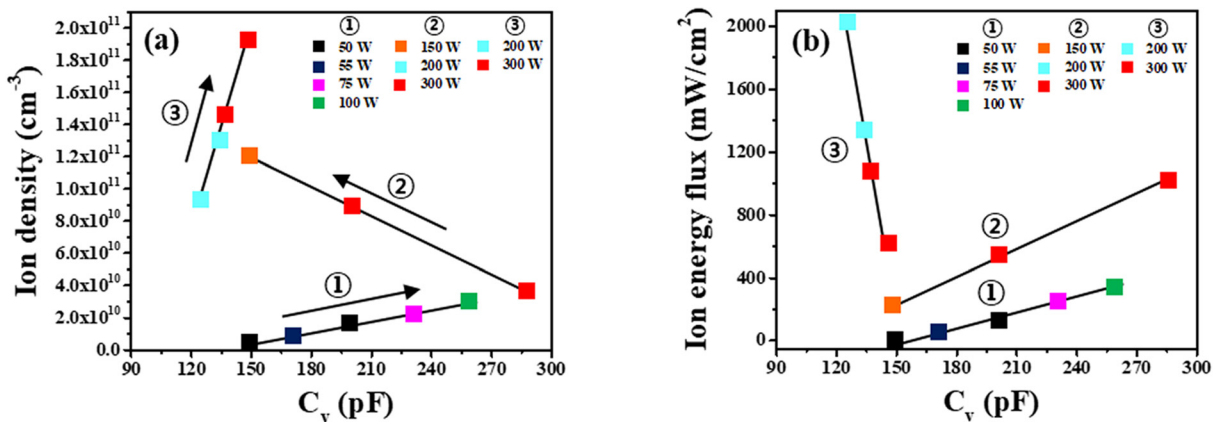

FIG. 6. (a) The linearly controlled ion densities from Fig. 4 and (b) ion energy flux profiles as a function of C_v at 13.3 Pa (100 mTorr).
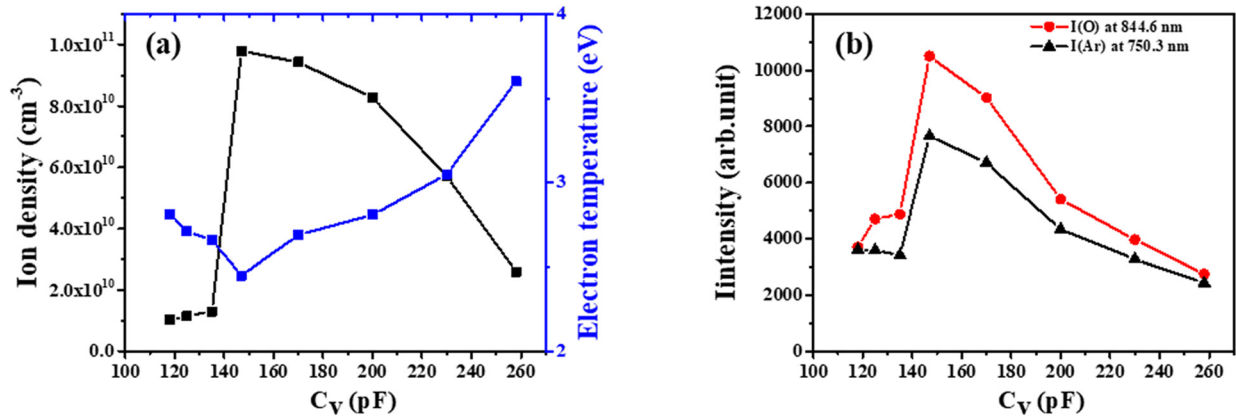
FIG. 7. (a) Ion density and electron temperature and (b) O 844.6 nm and Ar 750.4 nm emission intensities as a function of C_v at a fixed RF power of 300 W and 13.3 Pa (100 mTorr) in an oxygen plasma. Flow rates (sccm) are O_2:TRG = 20:1. (TRG = trace rare gas).

and the electron temperature as a function of C_v at 100 mTorr and 300 W in an oxygen plasma is shown in Fig. 7(a). When the series LC resonance occurs at 148 pF, a density jump occurs due to the E to H mode transition. Concurrently, the electron temperature is minimized, and the ion density is maximized. At the series LC resonance, the V_{CCP} is minimized, as shown in Fig. 3(f). The sheath voltage V_s is closely related to the V_{CCP} and is also minimized at resonance. Since the V_s is minimized, the ion acceleration loss is reduced, and the plasma potential is also minimized. Thus, the T_e is lowest at 148 pF.[33] Figure 7(b) shows the emission intensities of the O (844.6 nm) and Ar (750.4 nm) lines that are maximized at the series LC resonance. The emission intensities show similar behavior to the ion density as a function of C_v.

To evaluate the control of the O atom generation using the hybrid plasma source, the O atom (3p ^{3}P, 844.6 nm, E = 10.94 eV) number density was obtained from the measured intensity peaks of light emission by using OES actinometry. The intensity of optical emission lines of the oxygen hybrid discharge is recorded by a spectrometer (HR4000, Ocean optics Inc.), yielding a spectral resolution of 0.5 nm/FWHM. The hybrid plasma is optically thin, and the light is collected by the optical probe. Figure 8 shows a sample optical emission spectrum, covering the 700–860 nm wavelength range, of an oxygen plasma for different values of C_v. Ar emission lines emerged at various wavelengths, including 750.4, 763.5, 794.8, and 811.5 nm, and O atom peaks were visible near 777.4 nm and at 844.6 nm. The emission intensity of the 750.4 nm Ar (2p$_1$, E = 13.48 eV) line is a good pair for the energy of emitting levels of 844.6 nm O atom line and is not affected by the electron impact out of metastable states.[34,35] The emission intensities are changed by adjusting C_v. When the series LC resonance occurs, the emission intensities of both the 844.6 nm O and 750.4 nm Ar lines are maximized.

Figure 9 shows the O-to-Ar number density ratios as a function of C_v. The O-to-Ar number density ratio is given by[36–40]

$$\frac{n_O}{n_{Ar}} = \frac{k_{Ar}}{k_O} \frac{b_{Ar}}{b_O} \frac{\gamma_{Ar}}{\gamma_O} \frac{I_O}{I_{Ar}}, \tag{9}$$

where the rate coefficients, k_{Ar} and k_O, for the electron impact excitation from the ground states and the rate coefficient expressions $k_{Ar} = 2.48 \times 10^{-14} T_e 0.33 \exp(-12.78/T_e)$ and $k_O = 7.1 \times 10^{-9} \exp$

$(-8.6/T_e)$ m^3 s^{-1}.[25,41] The optical branching ratio, b_{Ar} and b_O, for the emitting states at the monitored wavelengths is $b_{Ar}/b_O = 1$.[42–44] The spectral response corrections, γ_{Ar} and γ_O, are relative sensitivities of the spectrometer at the wavelengths where the species and actinometer emit for the spectrometer employed, which is 2.5.[39,40] In this work, effects of the self-absorption are neglected.[45,46] At the series LC resonance, n_O/n_{Ar} is maximized and is controlled by adjusting C_v. This experiment result shows that the hybrid plasma source controls O atom generation at a fixed pressure and applied power. This feature is a unique advantage of the hybrid plasma source. Further, our hybrid plasma source can be applied to processing plasmas, such as in the ashing process of a photoresistor (PR) and in plasma dry cleaning.

V. CONCLUSION

We developed a hybrid plasma source that combines an ICP source and a CCP source in parallel using a single RF power generator. The currents flowing through each source were controlled by a variable capacitor connected to the antenna in the ICP section. To
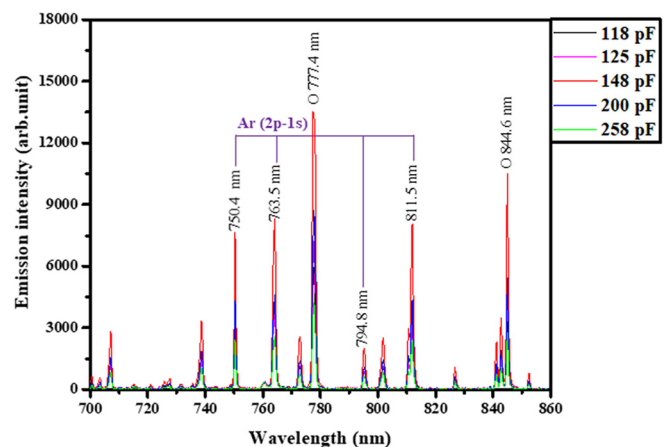

FIG. 8. Optical emission spectrum from 700 to 860 nm at a fixed RF power of 300 W and 13.3 Pa (100 mTorr) in an oxygen plasma. Flow rates (sccm) are O_2:TRG = 20:1. TRG = trace rare gas.
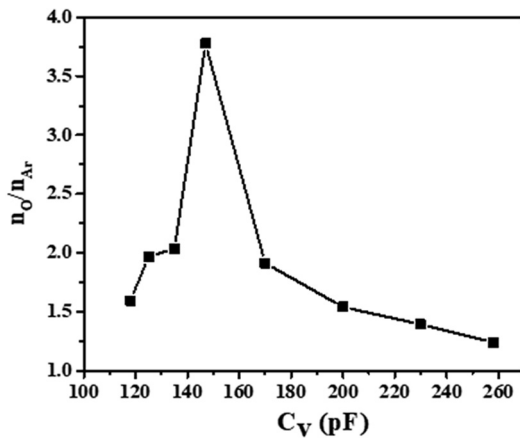
FIG. 9. n_O/n_{Ar} number density ratio as a function of C_v at a fixed RF power of 300 W and 13.3 Pa (100 mTorr) in an oxygen plasma. Flow rates (sccm) are O_2:TRG = 20:1. TRG = trace rare gas.

investigate the characteristics of the proposed hybrid source, the electrical properties and the plasma parameters were measured. The electrical characteristics of the voltage and current flowing through each source can be controlled by adjusting the C_v at a fixed applied power. The ion density showed different trends depending on the discharge mode. In E-mode, the ion density was governed by the CCP current, whereas it was controlled by the ICP current in H-mode. These results show that a large discrepancy of the absolute value with the calculated plasma density from the power balance equation is in good qualitative agreement. Using the variable capacitor, a wide range of the ion densities were obtained at a fixed applied power. Interestingly, the ion density was controlled linearly at 13.3 Pa (100 mTorr) by adjusting power dissipation, which is a very unique feature of our hybrid plasma source. This type of control is impossible in conventional ICPs due to the E–H transition. In addition, OES actinometry method verified that our source was capable of controlling O atom generation. Our plasma source can be applied to plasma processing applications where ion density control and stable plasma operation are important such as O atom generation for dry cleaning or dry treatment.

ACKNOWLEDGMENTS

DATA AVAILABILITY

The data that support the findings of this study are available from the corresponding author upon reasonable request.

REFERENCES

[1]J. Hopwood, Plasma Sources Sci. Technol. **1**, 109 (1992).
[2]J. H. Keller, Plasma Sources Sci. Technol. **5**, 166 (1996).
[3]D. B. Graves, IEEE Trans. Plasma Sci. **22**, 31 (1994).
[4]U. Kortshagen, N. D. Gibson, and J. E. Lawler, J. Phys. D **29**, 1224 (1996).
[5]K. Suzuki, K. Nakamura, H. Ohkubo, and H. Sugai, Plasma Sources Sci. Technol. **7**, 13 (1998).
[6]K. Chandrakar, J. Phys. D **11**, 1809 (1978).
[7]G. A. Hebner, E. V. Barnat, P. A. Miller, A. M. Paterson, and J. P. Holland, Plasma Sources Sci. Technol. **15**, 879 (2006).
[8]M. Surendra and D. B. Graves, Appl. Phys. Lett. **59**, 2091 (1991).
[9]P. Chabert and N. Braithwaite, *Physics of Radio-Frequency Plasmas* (Cambridge University Press, 2011).
[10]H. X. Li, T. Xu, J. M. Chen, H. D. Zhou, and H. W. Liu, Appl. Surf. Sci. **227**, 364 (2004).
[11]Y. H. Lee, K. K. Chan, and M. J. Brady, J. Vac. Sci. Technol., A **13**, 596 (1995).
[12]A. Hallil, O. Zabeida, M. R. Wertheimer, and L. Martinu, J. Vac. Sci. Technol., A **18**, 882 (2000).
[13]C. M. Compagnoni, A. Goda, A. S. Spinelli, P. Feeley, A. L. Lacaita, and A. Visconti, Proc. IEEE **105**(9), 1609–1633 (2017).
[14]R. A. Ovanesyan, E. A. Filatova, S. D. Elliott, D. M. Hausmann, D. C. Smith, and S. Agarwal, J. Vac. Sci. Technol., A **37**(6), 060904 (2019).
[15]C. Han, Z. Wu, C. Yang, L. Xie, B. Xu, L. Liu, Z. Yin, L. Jin, and Z. Huo, Semicond. Sci. Technol. **35**, 045003 (2020).
[16]D. S. Han, H. C. Lee, H. J. Kim, Y. S. Kim, C. W. Chung, and H. S. Chae, Plasma Sources Sci. Technol. **22**, 055011 (2013).
[17]K.-I. Takagi, A. Ikeda, T. Fujimura, and Y. Kuroki, Thin Solid Films **386**, 160–164 (2001).
[18]H. C. Lee and C. W. Chung, Plasma Sources Sci. Technol. **24**, 024001 (2015).
[19]J. S. Kim, J. W. Bae, H. J. Kim, N. E. Lee, G. Y. Yeom, and K. H. Oh, Thin Solid Films **377-378**, 103–108 (2000).
[20]M. H. Lee, S. H. Jang, and C. W. Chung, J. Appl. Phys. **101**, 033305 (2007).
[21]J. Hopwood, Plasma Sources Sci. Technol. **3**, 460 (1994).
[22]V. A. Godyak and R. B. Piejak, J. Vac. Sci. Technol., A **8**, 3833-7 (1990).
[23]J. Y. Bang, A. Kim, and C. W. Chung, J. Appl. Phys. **107**, 103312 (2010).
[24]R. B. Piejak, V. A. Godyak, and B. M. Alexandrovich, Plasma Sources Sci. Technol. **1**, 179–186 (1992).
[25]M. A. Lieberman and A. J. Lichtenberg, *Principles of Plasma Discharges and Materials Processing* (Wiley, New York, 2005).
[26]V. Lisovskiy, J.-P. Booth, K. Landry, D. Douai, V. Cassagne, and V. Yegorenkov, Europhys. Lett. **82**, 15001 (2008).
[27]N. Jeanvoine, "Plasma-material interaction and electrode degradation in high voltage ignition discharges," Ph.D. thesis (University of Saarbrucken, Germany, 2009).
[28]Y. D. Kim, H. C. Lee, and C. W. Chung, Phys. Plasmas **20**, 093508 (2013).
[29]M. H. Lee and C. W. Chung, Phys. Plasmas **13**, 063510 (2006).
[30]J. H. Moon, H. J. Moon, and C. W. Chung, Phys Plasmas **26**, 093505 (2019).
[31]M. H. Lee, K. H. Lee, D. S. Hyun, and C. W. Chung, Appl. Phys. Lett. **90**(19), 191502 (2007).
[32]E. A. Kralkina, P. A. Nekliudova, V. B. Pavlov, A. K. Petrov, and K. V. Vavilin, Plasma Sources Sci. Technol. **26**, 055006 (2017).
[33]S. H. Seo, J. I. Hong, and H. Y. Chang, Appl. Phys. Lett. **74**, 2776 (1999).
[34]J. B. Boffard, G. A. Piech, M. F. Gehrke, L. W. Anderson, and C. C. Lin, Phys. Rev. A **59**, 2749 (1999).
[35]J. W. Coburn and M. Chen, J. Appl. Phys. **51**, 3134 (1980).
[36]R. E. Walkup, K. L. Saenger, and G. S. Selwyn, J. Chem. Phys. **84**(5), 2668–2674 (1986).
[37]D. Pagnon, J. Amorim, J. Nahorny, M. Touzeau, and M. Vialle, J. Phys. D **28**, 1856 (1995).
[38]N. C. M. Fuller, M. V. Malyshev, V. M. Donnelly, and I. P. Herman, Plasma Sources Sci. Technol. **9**(2), 116–127 (2000).
[39]E. Karakas, V. M. Donnelly, and D. J. Economou, J. Appl. Phys. **113**, 213301 (2013).
[40]Q. Lou, S. Kaler, V. M. Donnelly, and D. J. Economou, J. Vac. Sci. Technol., A **33**, 021305 (2015).
[41]J. T. Gudmundsson, I. G. Kouznetsov, K. K. Patel, and M. A. Lieberman, J. Phys. D **34**, 1100–1109 (2001).
[42]K. Niemi, V. Schulz-von der Gathen, and H. F. Döbele, Plasma Sources Sci. Technol. **14**, 375 (2005).
[43]Y. K. Lee, S. Y. Moon, S. J. Oh, and C. W. Chung, J. Phys. D **44**, 285203 (2011).
[44]H. M. Katsch, A. Tewes, E. Quandt, A. Goehlich, T. Kawetzki, and H. F. Dobele, J. Appl. Phys. **88**(11), 6232 (2000).
[45]N. Konjević, Phys. Rep. **316**, 339 (1999).
[46]D. V. Lopaev, A. V. Volynets, S. M. Zyryanov, A. I. Zotovich, and A. T. Rakhimov, J. Phys. D **50**, 075202 (2017).